

Delocalization Error and “Functional Tuning” in Kohn–Sham Calculations of Molecular Properties

Jochen Autschbach^{*,†} and Monika Srebro[‡]

[†]Department of Chemistry, University at Buffalo, State University of New York, Buffalo, New York 14260-3000, United States

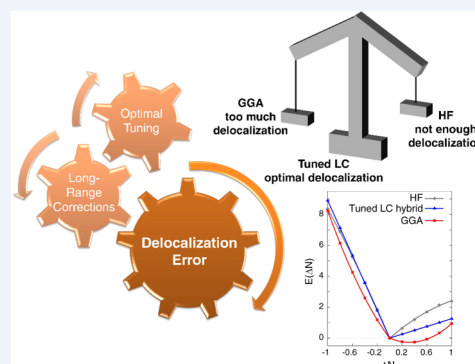
[‡]Department of Theoretical Chemistry, Faculty of Chemistry, Jagiellonian University, R. Ingardena 3, 30-060 Krakow, Poland

S Supporting Information

CONSPECTUS: Kohn–Sham theory (KST) is the “workhorse” of numerical quantum chemistry. This is particularly true for first-principles calculations of ground- and excited-state properties for larger systems, including electronic spectra, electronic dynamic and static linear and higher order response properties (including nonlinear optical (NLO) properties), conformational or dynamic averaging of spectra and response properties, or properties that are affected by the coupling of electron and nuclear motion.

This Account explores the sometimes dramatic impact of the delocalization error (DE) and possible benefits from the use of long-range corrections (LC) and “tuning” of functionals in KST calculations of molecular ground-state and response properties. Tuning refers to a nonempirical molecule-specific determination of adjustable parameters in functionals to satisfy known exact conditions, for instance, that the energy of the highest occupied molecular orbital (HOMO) should be equal to the negative vertical ionization potential (IP) or that the energy as a function of fractional electron numbers should afford straight-line segments. The presentation is given from the viewpoint of a chemist interested in computations of a variety of molecular optical and spectroscopic properties and of a theoretician developing methods for computing such properties with KST. In recent years, the use of LC functionals, functional tuning, and quantifying the DE explicitly have provided valuable insight regarding the performance of KST for molecular properties.

We discuss a number of different molecular properties, with examples from recent studies from our laboratory and related literature. The selected properties probe different aspects of molecular electronic structure. Electric field gradients and hyperfine coupling constants can be exquisitely sensitive to the DE because it affects the ground-state electron density and spin density distributions. For π -conjugated molecules, it is shown how the DE manifests itself either in too strong or too weak delocalization of localized molecular orbitals (LMOs). Optical rotation is an electric–magnetic linear response property that is calculated in a similar fashion as the electric polarizability, but it is more sensitive to approximations and can benefit greatly from tuning and small DE. Hyperpolarizabilities of π -conjugated “push–pull” systems are examples of NLO properties that can be greatly improved by tuning of range-separated exchange (RSE) functionals, in part due to improved charge-transfer excitation energies. On-going work on band gap predictions is also mentioned. The findings may provide clues for future improvements of KST because different molecular properties exhibit varying sensitivity to approximations in the electronic structure model. The utility of analyzing molecular properties and the impact of the DE in terms of LMOs, representing “chemist’s orbitals” such as individual lone pairs and bonds, is highlighted.



1. BACKGROUND

1.1. Kohn–Sham Theory (KST)

Quantum-theoretical predictions of molecular properties require treating electron correlation. In wave function theory (WFT), the computational effort for increasing accuracy scales with increasing powers of the system size, such that WFT remains impractical for many systems of interest in chemistry, biochemistry, or materials science. KST in its original form¹ relies on the molecular energy being a universal functional of the electron density, $\rho(\mathbf{r})$, and the orbitals are calculated from a (semi)local potential. In more general KST, the potential may also be nonlocal and explicitly depend on orbitals and other quantities. Approximations are developed within these

paradigms. Perdew² alludes to a ladder of functionals reaching “quantum-mechanical heaven”, where each rung represents a better performing class of functionals: LDA (rung 1), GGA (2), hybrid GGA (3), and so forth.

Within this hierarchy, static molecular properties can be calculated as KST energy derivatives. Time-dependent (TD) KST³ gives access to dynamic (frequency-dependent) properties. There are, however, many cases where the performance of approximate KST is wanting.⁴ For molecular response properties, the problems are frequently severe. An example is the sometimes dramatic underestimation of charge-transfer

Received: April 28, 2014

Published: June 26, 2014

(CT) excitation energies by TD-KST linear response.^{4–6} Examples are given in Figure 1 and Table 1. Poor performance

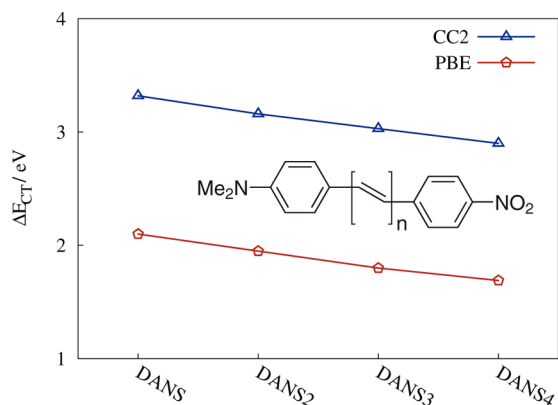


Figure 1. CT excitation energies for (*E*)-*N,N*-dimethyl-4-(4-nitrostyryl)aniline (DANS, $n = 1$) and related systems. Approximate coupled-cluster (CC2) vs KST/PBE linear response.⁷

Table 1. CT Excitation Energies (eV) for Aryl–Tetracyanoethylene Complexes, after Stein et al.¹⁵

aryl	B3LYP	BNL	IP-tuned BNL	expt
benzene	2.1	4.4	3.8	3.6
toluene	1.8	4.0	3.4	3.4
<i>o</i> -xylene	1.5	3.7	3.0	3.2
naphthalene	0.9	3.3	2.7	2.6

for electronic spectra and other response properties are related, because the latter can be written as “sum-over-states” (SOS) depending on excitation energies and transition moments.

Failures for response properties and spectra go along with a wrong asymptotic behavior of approximate exchange–correlation (XC) potentials V_{XC} for isolated molecules, “nearsightedness” of XC response kernels, and lack of the integer discontinuity.^{2,8} There is a connection⁹ between TD-KST failures and the adiabatic approximation used in practically all calculations of dynamic properties and spectra. The asymptotic behavior of the (nonlocal) potential experienced by an electron is correct in HF theory. HF is also one-electron self-interaction free. These features of HF theory stem from the exact cancellation of orbital self-Coulomb repulsion by self-exchange in the energy and the potential.

1.2. Range Separation

In KST with long-range corrected (LC) functionals, the electron repulsion, r_{12}^{-1} , is range-separated in the exchange¹⁰ and switches to exact exchange (eX) for large r_{12} . This gives an asymptotically correct potential. A flexible three-parameter expression¹¹ is

$$\frac{1}{r_{12}} = \frac{1 - [\alpha + \beta \operatorname{erf}(\gamma r_{12})]}{r_{12}} + \frac{\alpha + \beta \operatorname{erf}(\gamma r_{12})}{r_{12}} \quad (1)$$

γ is the range-separation parameter, with typical values of 0.3–0.5 au in globally parametrized range-separated exchange (RSE) functionals using an erf separation. For molecular applications, the long-range term is the second on the right-hand side; α then quantifies the fraction of eX in the short-range limit, while $\alpha + \beta$ gives the eX fraction in the long-range limit. LC requires $\alpha + \beta = 1$.

LC hybrids can significantly improve CT excitations.^{11,12} However, not every CT excitation affords large spatial separations of the orbitals. In a Coulomb-attenuated method (CAM),¹¹ the LC is incomplete. The CAM-B3LYP functional affords $\alpha + \beta = 0.65$. Global parametrizations of RSE functionals designed for CT excitations are not necessarily accurate for other properties, and the performance is sensitive to the choice of α , β , and γ .¹³

1.3. Optimal Tuning

The parameter γ is a functional of the density and should be system-dependent.¹⁴ A nonempirical “tuning” was proposed whereby γ is chosen system-specifically such that the HOMO energy, ϵ_H , matches $-IP$. This is a condition of exact KST. Impressively good excitation energies were calculated for CT complexes via tuning of the BNL functional,¹⁵ as shown in Table 1. Improved performance of tuned LC functionals over standard functionals or RSE functionals with fixed global parametrizations has since been demonstrated for CT and “CT-like” excitations and other energy gaps.^{14,16–19}

1.4. Delocalization Error (DE)

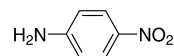
The exact KST energy $E(N)$ varies linearly² for electron numbers N between integers N_i . In the absence of explicit ensemble treatment, approximate functionals do not generally produce straight-line segments for $E(N)$ for molecules, even if the $E(N_i)$ are quite accurate. Instead, there may be pronounced curvature in $E(N)$. This curvature indicates the DE.⁴ There is a close relationship between the DE and the one- and many-electron self-interaction error. Positive curvature (convex behavior) indicates an unphysically strong electron delocalization, which is typically obtained with standard functionals. Negative curvature (concave behavior) indicates too strong localization, which is typically obtained with hybrids with large fractions of eX and HF. The DE directly affects calculated chemical and physical properties of molecules, since one may consider covalency as a form of electron delocalization. LC functionals tend to produce comparatively small $E(N)$ curvature²⁰ and therefore, presumably, small DEs. This improves further upon IP-tuning,^{21,22} but the severity of the DE may also depend critically on the eX in the short-range part,²³ that is, on α in eq 1.

1.5. Scope

In 2009, one of us took the opportunity to highlight the “tuning” results of ref 15,⁶ noting that an “open question is whether [tuning] will help to improve (or at least not deteriorate) other computed properties”. In recent years, our research group has explored the performance of tuned RSE hybrid functionals for “other computed properties” and the impact of the DE thereupon. Herein, we discuss selected ground-state and response properties, how they are impacted by the DE, and whether tuning gives improved results. With or without tuning, the DE is easily quantified and, along with LMO analyses of properties, instructive for diagnosing problems in KST calculations.

2. IP-TUNING AND DE MINIMIZATION WITH RSE HYBRIDS

To illustrate the discussion in this section, calculations are presented for *para*-nitroaniline (p-NA).⁷ p-NA is a π -



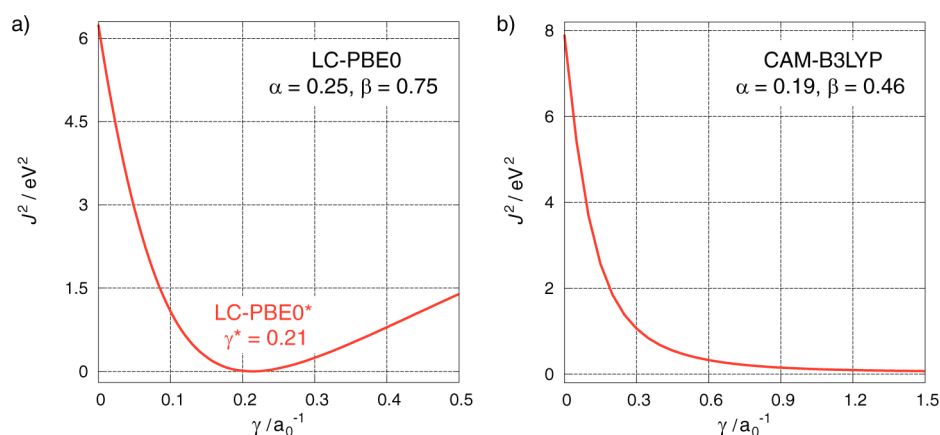


Figure 2. p-NA. J^2 versus γ calculated with two RSE functionals. No minimum of J^2 was found with CAM-B3LYP even for $\gamma > 1.5$.

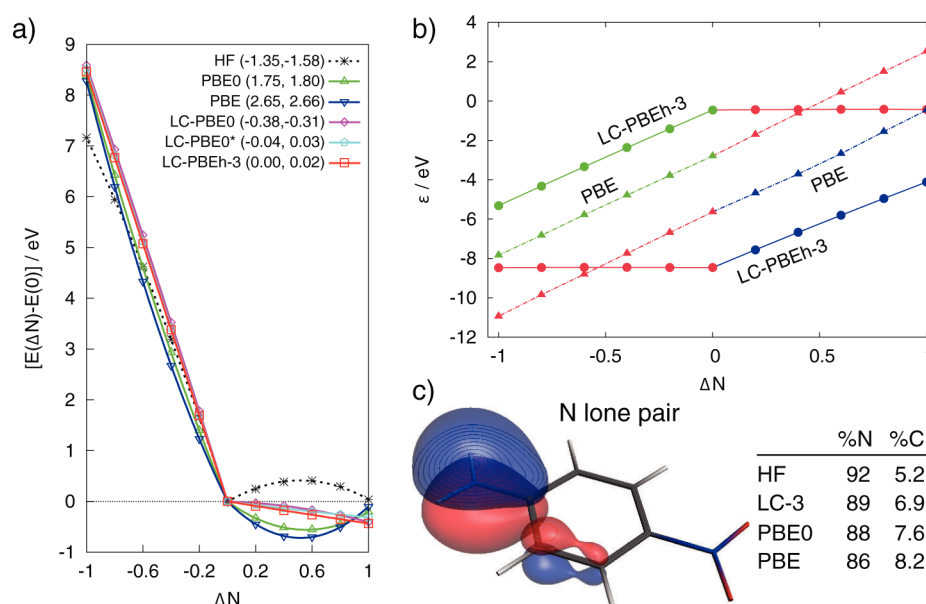


Figure 3. p-NA. (a) $E(\Delta N)$, numerical values in parentheses are curvatures for $\Delta N < 0$ and $\Delta N > 0$, indicating the DE. (b) Orbital energies for HOMO - 1 (blue), HOMO (red), and LUMO (green) versus ΔN . (c) Amine N lone-pair LMO. Percentage of the electron density associated with N and the neighboring carbon, from an NBO analysis. LC-3 is the 2DT parametrization no. 3 from Figure 4.

conjugated “push–pull” chromophore frequently used as a benchmark system for molecular response properties. p-NA has a strong physically meaningful π -delocalization assisting the push–pull mechanism and a lowest-energy π – π^* excitation with some CT character. The Supporting Information provides full details.

IP-tuning is based on the exact KST condition:^{2,4}

$$\varepsilon_{\text{H}}(N_0) + \text{IP}(N_0) = 0 \quad (2)$$

N_0 indicates a reference electron number of the target system. With an approximate RSE functional, ε_{H} and IP strongly depend on γ of eq 1. One can therefore try finding a molecule-specific γ nonempirically to satisfy eq 2, with ε_{H} and $\text{IP} = E(N_0 - 1) - E(N_0)$ calculated with the same functional.¹⁴ The corresponding γ^* value determines the IP-tuned functional.

The same value of γ^* may not satisfy eq 2 equally well for different N . One may therefore minimize¹⁶

$$J^2 = \sum_i [\varepsilon_{\text{H}}(N_0 + i) + \text{IP}(N_0 + i)]^2 \quad (3)$$

or another suitable measure. Most commonly, $i = 0, 1$, such that the HOMOs of the N_0 - and $(N_0 + 1)$ -electron species are simultaneously IP-tuned to the best degree possible.

Pioneering tuning studies employed LC functionals with $\alpha = 0$ learning γ as the only adjustable parameter. An RSE functional may also be IP-tuned successfully for $\alpha \neq 0$,^{21,23} but we found for molecules that the functional should afford $\alpha + \beta = 1$ (LC) likely for reasons outlined in the Supporting Information. Figure 2 demonstrates successful IP-tuning of LC-PBE0. No minimum of J^2 is found for the CAM-B3LYP functional (65% eX asymptotically). For p-NA, γ^* is much smaller than typical LC functional values of 0.3–0.5, meaning a switch to eX at larger r_{12} . This is often found for larger π -conjugated molecules.^{7,17,24,25}

Plots of $E(N)$ may diagnose the DE. Figure 3a demonstrates the deviations from the ideal straight-line segment behavior for p-NA from calculations with noninteger N . The coefficients of $(\Delta N)^2$ from quadratic fits of $E(\Delta N)$ with $\Delta N = N - N_0$ provide numerical measures of the curvature. The results for p-NA reflect typical trends: HF produces insufficient delocalization, while the positive curvatures obtained with most KST

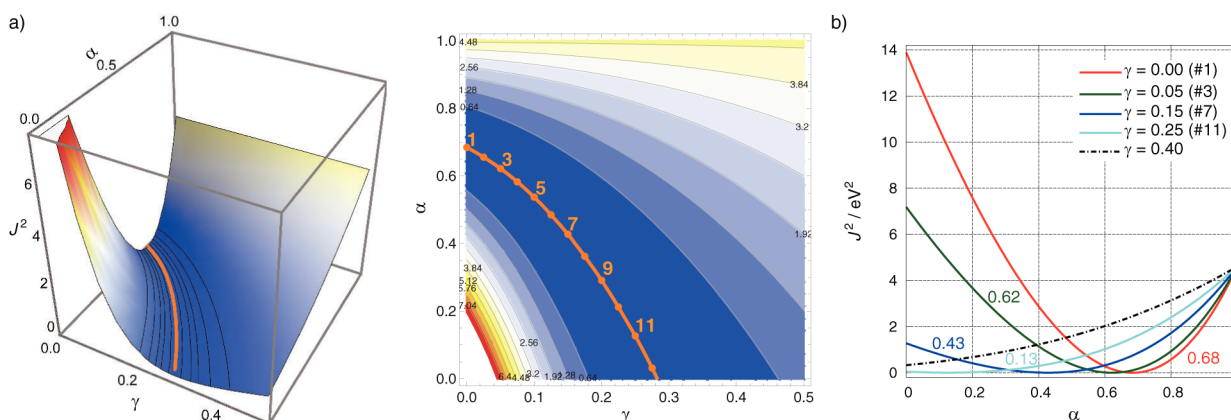


Figure 4. p-NA. Two-dimensional tuning of LC PBE hybrid. (a) 3D and contour plot of J^2 (eV^2) vs γ and $\alpha = 1 - \beta$. The thick (orange) line corresponds to $J^2 \approx 0$ along which 12 parametrizations were chosen to find minimal DE. (b) J^2 versus α for fixed γ . The optimal α are listed.

calculations indicate overdelocalization. See ref 26 for a way to approximate $E(N)$ curves without performing calculations with fractional electron numbers.

There are well-established procedures to localize molecular orbitals spatially as best as possible for a given density matrix. How well the LMOs can be localized depends on the extent of physically meaningful delocalization and also on the DE. For p-NA, the extent and sign of the DE is mirrored by the delocalization of the amine nitrogen π lone-pair (LP) onto the aryl moiety. Note the large *relative* variation of %C in Figure 3. For HF, $\pi\text{LP}(N)$ from an NBO calculation has 5% of its density on the neighboring carbon atom. Due to the negative DE, this number does not reflect the physically meaningful extent of the π -delocalization of p-NA. PBE gives a carbon percentage of 8%. Due to the large positive DE, the $\pi\text{LP}(N)$ is too strongly delocalized with PBE.

Vydrov et al.²⁰ conjectured that there is some value of γ for a given RSE functional and molecule producing a straight-line behavior of $E(\Delta N)$. Such a value may be determined approximately via IP-tuning.^{21,22} As seen in Figure 3a, LC-PBE0 with a typical $\gamma = 0.3$ already gives a much smaller DE than most other calculations, but the DE improves further with the IP-tuned version from Figure 2.

The range separation in eq 1 has three adjustable parameters, reduced to two unknowns by requiring LC, that is, $\beta = 1 - \alpha$. Figure 4 displays J^2 for p-NA on a two-dimensional α/γ grid, under the LC constraint. The orange line in the valley indicates an essentially continuous range of parameter sets for which $J^2 \approx 0$. But which one is the “best”? We proposed a *two-dimensional tuning*²³ (2DT) as a generalization of the one-dimensional IP-tuning. Within the tunable α/γ sector, IP-tuned parameter sets are selected, and the DE for each is probed. A 2DT functional minimizes J^2 and has the smallest $E(N)$ curvature. We note that the two criteria, while not the same, are interrelated. One could also set out to minimize curvature in the α/γ space and find that the resulting parametrization(s) have small J^2 . For p-NA, 2DT unambiguously leads to parametrization no. 3 of Figure 4. The situation may not always be as clear-cut as seen for $\text{Fe}(\text{acac})_3$ in section 3. 2DT may be necessary for KST calculations of molecular properties that are particularly sensitive to the DE. As shown in the Supporting Information, IP-tuning and DE minimization may, however, go along with an increase of the static correlation error⁴ (SCE), while for p-NA the functionals with the largest DE exhibit smaller SCE.

Janak’s theorem⁴ implies that $dE/dN = \varepsilon_{\text{H}}(N)$. Combined with the straight-line segment behavior of $E(N)$, this means that $\varepsilon_{\text{H}}(N)$ should be constant between integers and equal to $-\text{IP}(N_i)$ of the species with next higher integer N_i . When passing through N_i , there is a “jump” in ε_{H} because the slope of $E(N)$ changes discontinuously, and ε_{H} changes to $-\text{IP}(N_{i+1}) = -\text{EA}(N_i)$. In the absence of any integer discontinuities in V_{XC} , the jump simply indicates that a different orbital becomes the HOMO. If the LUMO energy $\varepsilon_{\text{L}}(\Delta N < 0)$ makes a smooth transition to $\varepsilon_{\text{H}}(\Delta N > 0)$ and if the straight-line segment behavior of $E(N)$ is satisfied, at $N = N_0$ the orbital energy gap should be equal to the calculated $\text{IP}(N_0) - \text{EA}(N_0)$. As seen in Figure 3b for p-NA, the 2DT LC hybrid functional delivers such a behavior. The value of ε_{H} stays constant between integers and jumps at N_0 from $-\text{IP}(N_0)$ to $-\text{EA}(N_0)$. Numerically, $\varepsilon_{\text{L}}(N_0) - \varepsilon_{\text{H}}(N_0)$ is very close to $\text{IP}(N_0) - \text{EA}(N_0)$ (see Supporting Information). The situation is very different for PBE: $\varepsilon_{\text{H}}(\Delta N)$ is not constant, and at N_0 the orbital energy gap is only about 1/3 of $\text{IP} - \text{EA}$. The 2DT functional also gives an electronic excitation energy (“optical gap”) from TD-KST close to an accurate WFT reference value (Supporting Information). PBE0 and in particular PBE significantly underestimate this excitation energy due to its partial CT character.

3. CASE STUDIES

3.1. Electric Field Gradients (EFGs) at Transition Metal Centers

EFGs in molecules interact with nuclear quadrupole moments. This interaction is observed in various types of spectroscopy. Therefore, there has been a long-standing interest in calculating EFGs. The EFG depends directly on the ground-state electron charge density.²⁷ An accurate prediction of the EFG at transition metal centers has long been considered a difficult problem for KST.²⁷ A notorious example is the Cu EFG in the CuCl diatomic molecule, Table 2. Relativistic CC theory and experiment place the largest-magnitude EFG tensor element V_{33} at Cu around -0.3 au. The HF data indicate that the lack of electron correlation gives a much too strong polarization of the 3p shell. KST with most standard functionals does not even give the correct sign.

The electron density can be partitioned into densities of LMOs representing individual lone pairs, bonds, and core orbitals, which is very useful for analyzing EFGs. Table 2 gives an LMO breakdown of the Cu EFG. Figure 5 shows the

Table 2. CuCl:²³ LMO Analysis of Cu EFG (au)^a

LMO	HF	BLYP	B3LYP	LC-PBE0	LC-PBEh*
$\sigma(\text{Cl} \rightarrow \text{Cu})$	-0.456	-0.466	-0.449	-0.511	-0.482
Cu Σ s	-0.002	-0.051	-0.037	-0.030	-0.019
Cu Σ 2p	-0.036	0.086	0.056	0.032	0.010
Cu Σ 3p	-0.763	0.041	-0.162	-0.352	-0.472
Cu d_σ (ea.)	8.609	8.774	8.745	8.723	8.689
Cu d_π (ea.)	-4.256	-4.317	-4.306	-4.294	-4.282
Cu d_σ	-8.086	-7.569	-7.755	-7.898	-7.971
Cu Σ 3d	0.620	1.345	1.123	0.960	0.843
Cl Σ all	-0.238	-0.221	-0.224	-0.218	-0.225
total calcd ^b	-0.872	0.730	0.308	-0.120	-0.344
$\sigma(\text{Cl} \rightarrow \text{Cu})$					
% Cu	7.74	20.08	16.65	12.66	11.49
% p	4.34	0.59	1.13	2.87	3.04
% d_σ	2.22	7.76	5.68	4.33	3.46
% 4s in d_σ	1.81	8.05	5.79	4.29	3.33

^aLC-PBEh* = 2DT parametrization no. 4 of Figure 5. ^bRelativistic CC = -0.341, Experiment = -0.31(2), see ref 27.

significant DEs for CuCl measured by $E(N)$ curvature. The LMO analysis reflects the sign and magnitude of the DE very clearly. The Cu–Cl bond is predominantly ionic, with some dative covalent character reflected in the $\sigma(\text{Cl} \rightarrow \text{Cu})$ and Cu d_σ LMOs. Positive DE overestimates the covalency, as evident in the contributions of Cu atomic orbitals to $\sigma(\text{Cl} \rightarrow \text{Cu})$: 20% with BLYP but only 8% with HF. This percentage, the weight of p vs d_σ in $\sigma(\text{Cl} \rightarrow \text{Cu})$, and contributions from 3p that are coupled to the latter drive the EFG trend.

CuCl was subjected to 2DT. Although the $E(\Delta N)$ curvature is small for each of the IP-tuned functionals, the variations of the EFG are sizable.²³ The 2DT parametrization gives a balanced description of the electron density and an accurate EFG. Since the Cu EFG is exquisitely sensitive to the DE, only a functional giving nearly vanishing curvature is reliable. The EFGs of other simple Cu(I) compounds are also reproduced with the 2DT parametrization of CuCl,²³ indicating that 2DT for one molecule may be applicable to a class of similar compounds. Despite that the optimal 2DT parameters for CuCl are unlikely optimal for Cu and Cl, calculated atomization energies for the tuned parametrizations were in the range of 7.6–8.4 eV, not too far from the DK-CCSD(T) reference value

of 7.8 eV. For more severe size-consistency problems, see ref 28.

3.2. Spin Density Distributions and Hyperfine Coupling (hfc)

The total density is the sum of the \uparrow and \downarrow spin densities, $\rho = \rho^\uparrow + \rho^\downarrow$. The spin density $\rho^{\text{spin}} = \rho^\uparrow - \rho^\downarrow$ may also be affected by the DE. An important property depending on ρ^{spin} is electron–nucleus hfc, routinely measured in EPR. Our interest in hfc stems from its role in ligand NMR chemical shifts of paramagnetic metal complexes.²⁹ The *contact shifts* are proportional to the isotropic hfc for the nucleus in question, which is in turn proportional to ρ^{spin} at the nucleus. If ρ^{spin} in the ligand system originates at the metal center, it is nonzero because of covalent metal–ligand interactions. If the covalency is unphysically strong or weak because of the DE, this may lead to gross errors for hfc.

Fe(acac)₃ is a representative example from ref 29. A qualitative orbital diagram for the complex is presented in Figure 6. Due to the high-spin d^5 configuration, covalent oxygen-to-metal σ -donation can only occur via \downarrow orbitals. A secondary interaction (minor for Fe(acac)₃) is π -backbonding involving Fe \uparrow orbitals. Both interactions create an excess of \uparrow spin in the ligand system.

The DE was numerically assessed,²⁹ revealing the expected trends. The DE has a dramatic effect on the dative O \rightarrow Fe interactions (Table 3) but as anticipated only for \downarrow spin. The trend for the methyl carbon hfc follows the %Fe of iron orbitals in the donating oxygen LMOs, which in turn follows the DE trend. From HF to BP, the hfc increases by a factor of 4. One megahertz of isotropic ¹³C hfc corresponds to a paramagnetic NMR contact shift of about 1200 ppm,²⁹ that is, the impact of the DE on the NMR shifts is extremely severe.

The 2DT improved the $E(N)$ curvature and gave methyl carbon hfc between 1.8 and 1.3 MHz. However, J^2 for the IP-tuned parametrizations in Figure 7 increases from 0.003 eV² for the smallest α to 0.183 for the largest α , meaning that the tuning criteria cannot be satisfied well for larger α . Further, even with the smallest α the residual DE for Fe(acac)₃ is likely causing errors in the hfc. The parameter space of the functional may not be capable of producing an accurate electronic structure for Fe(acac)₃.

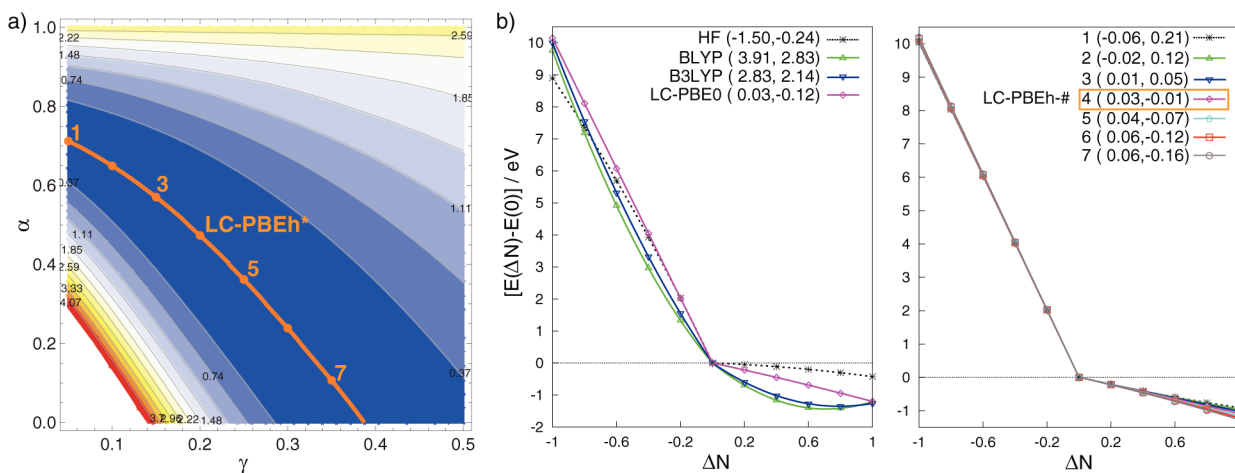


Figure 5. CuCl:²³ (a) J^2 , as in Figure 4. (b) $E(\Delta N)$ and curvature measures. (left) Standard functionals and HF. (right) Seven parametrizations from panel a. No. 4 = LC – PBEh* of Table 2 affords the least DE.

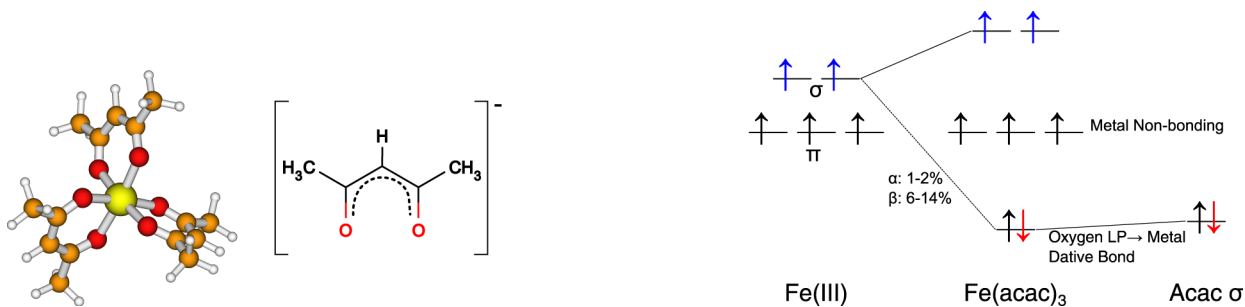


Figure 6. (left) A metal tris-acac complex. (right) Strongly simplified orbital diagram for $\text{Fe}(\text{acac})_3$. Dative covalent oxygen-metal σ -interactions may occur via \downarrow orbitals (red).

Table 3. $\text{Fe}(\text{acac})_3$:²⁹ Contribution of Iron Atomic Orbitals in the acac Oxygen σ -Donor Orbitals Separated by Spin, and Calculated ^{13}C hfc for the Acac Methyl Carbon

functional	BP	LC-PBE0	BHLYP	HF
%Fe in $\sigma(\text{O}\rightarrow\text{Fe})(\alpha)$	2	2	2	2
%Fe in $\sigma(\text{O}\rightarrow\text{Fe})(\beta)$	13	11	10	6
acac methyl ^{13}C hfc (MHz)	2.3	1.3	1.2	0.6

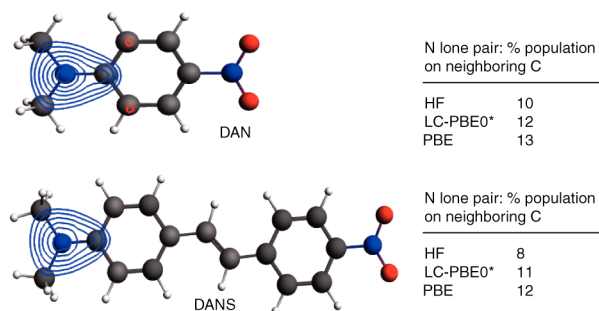


Figure 8. *N,N*-Dimethyl-4-nitroaniline (DAN) and DANS:⁷ Contour plots of the delocalized $\pi\text{LP}(\text{N})$ LMO (LC-PBE0*). Percentage of the donor N lone-pair density attributable to the neighboring carbon.

3.3. DE for π -Conjugated Chromophores

Quantifying the DE for organic π -conjugated chromophores can help to assess the performance of functionals in response property calculations and to get a sense of the “proper” extent of π -delocalization. Figure 8 shows $\pi\text{LP}(\text{N})$ LMOs of the Me_2N donor group of two push-pull chromophores. Strong π -delocalization and an intense low-energy CT excitation are design goals for such molecules. It is evident that both $\pi\text{LP}(\text{N})$ are delocalized toward the aromatic ring carbons.

Numerical studies⁷ showed for both molecules large $E(N)$ curvatures with HF and PBE and small DE with IP-tuned LC-PBE0*. Figure 8 lists the percentages of $\pi\text{LP}(\text{N})$ associated with the neighboring carbon. The relative extent of this delocalization is very sensitive to the DE, increasing by 50% for DANS when going from HF to PBE. Similar trends were demonstrated for π LMOs in the bridges.⁷ Presumably, LC-PBE0* produces a physically reasonable π -delocalization.

The extent of the DE goes in hand with the accuracy of the CT excitation energies, as demonstrated in Table 4 by comparison with two “affordable” WFT methods. See also Figure 1. Below, we discuss NLO properties for these molecules.

Cyanine dyes (Figure 9) afford strongly delocalized π -systems with very small bond-length alternations. Most TD-KST calculations significantly *overestimate* the lowest singlet excitation energies, with nonhybrid functionals getting close to accurate reference data.³⁰ One may wonder whether the DE has any bearing on the cyanine excitations. However, this is hardly the case. The apparently best performing functionals exhibit

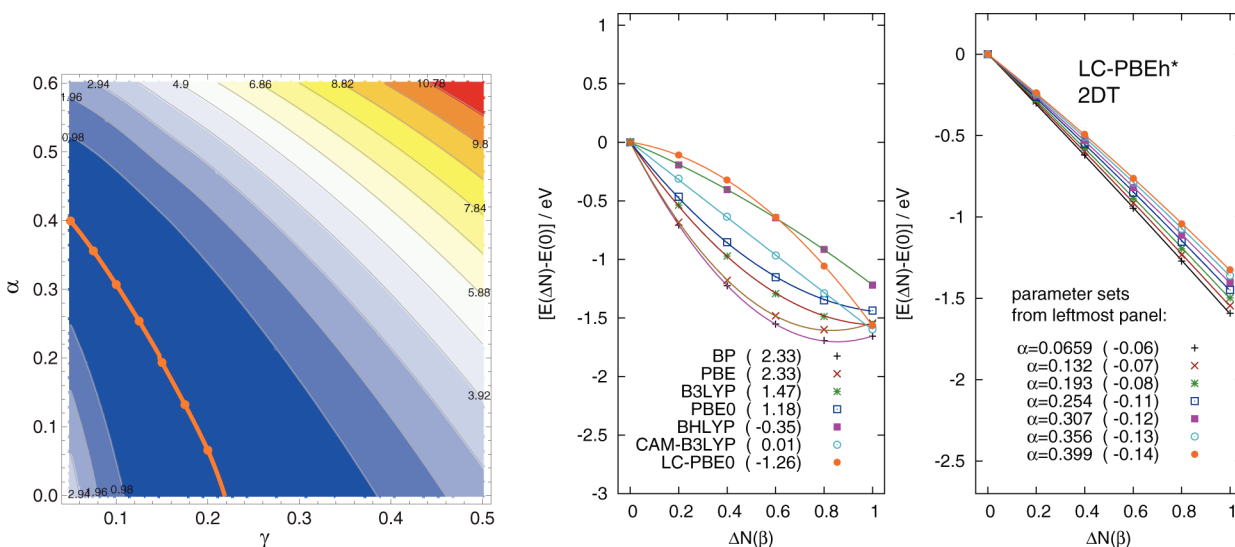
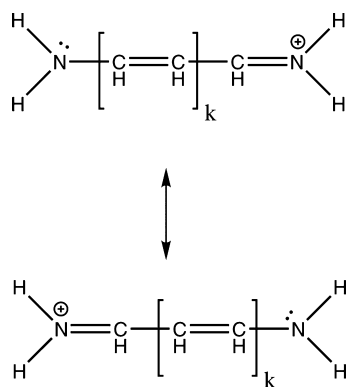


Figure 7. $\text{Fe}(\text{acac})_3$:²⁹ 2DT and assessment of the DE. Curvature measures in parentheses.

Table 4. Lowest-Energy π - π^* Excitation Energies (eV)^{7a}

	p-NA	DAN	DANS
HF	5.04	4.82	3.83
PBE	3.50	3.19	2.10
LC-PBE0*	4.44	4.08	3.32
CC2	4.39	3.94	3.32
CIS(D)	4.57	4.15	3.66

^aCT character increases as p-NA \lesssim DAN < DANS.

Figure 9. Linear cyanines, $k = 0, 1, 2, \dots$

significant DE.³¹ Instead, differential correlation between the excited state and the ground state is large and not reproduced by most functionals. Part of the problem is the separation of the singlet and triplet excitation energies (S/T), which is strongly overestimated by TD-KST because a large HOMO–LUMO eX integral is not sufficiently corrected by correlation from the XC response kernel. The “better” performance of nonhybrid functionals is likely nothing more than compensation of a “CT-like” problem in the triplet excitations by an overestimated S/T separation.

3.4. Long-Range Exciton Coupling and Exciton Circular Dichroism (CD)

The performance of TD-KST for the prediction of strong long-range exciton coupling has been investigated,²² motivated by experimental reports of exciton CD due to coupling of tetraphenylporphyrin (TPP) excitations in a derivatized natural product, brevetoxin-D (BTX-D), at distances upward of 40 Å.³² TPP has an intense Soret peak around 3 eV facilitating this coupling.

In ref 22, TPP₂ was considered after removing the brevetoxin linker. LC functionals delivered acceptable TD-KST electronic spectra for the TPP monomer and dimer and improved Soret band energies upon IP-tuning. TD-KST spectral data of the TPP monomer were used to simulate the exciton coupling with a dipole coupling model (matrix method, MM), producing excellent agreement with full dimer calculations but only for the LC functionals. Figure 10 compares the MM spectra with the experimental bis-TPP–brevetoxin spectrum. For MM(BP), the low-energy “tail” is caused by exciton coupling of spurious transitions contaminating the monomer spectrum. Their occurrence goes along with a significant DE. The spectrum based on the tuned LC functional is far superior. Likely reasons for the experimental low-energy intensity are the presence of the brevetoxin linker, dynamics of the system, and solvent–solute interactions.

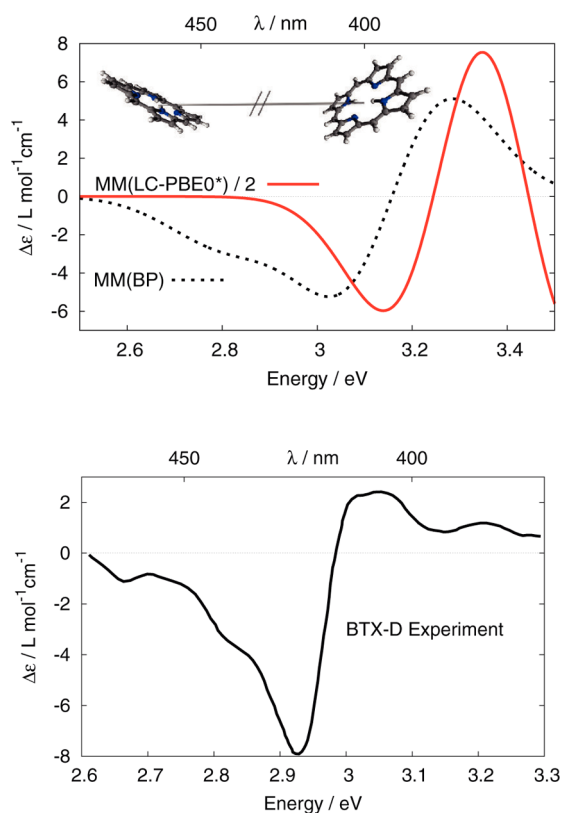


Figure 10. (top) Exciton coupling CD for TPP₂ at 42 Å separation, using monomer TD-KST spectra in a dipole coupling model (MM).²² (bottom) Experimental CD spectrum of TPP₂-BTX-D.³² Despite the apparently good match with experiment, the BP-based spectrum is seriously deficient.

3.5. Optical Rotation (OR)

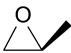
The absolute configuration of a chiral molecule can be determined by comparing the signs of calculated and measured chiroptical properties³³ such as optical rotation (OR) and CD. The SOS expression for the molecular OR parameter β reads

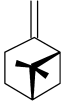
$$\beta(\omega) = \frac{2c}{3} \sum_{j \neq 0} \frac{R_j}{\omega_j^2 - \omega^2} \quad (4)$$

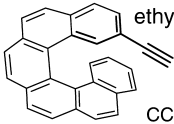
The observed molar rotation $[\phi]$ is proportional to $\omega^2 \beta$.³⁴ Here, $R_j = \text{Im}[\mathbf{D}_j \cdot \mathbf{M}_j^*]$ (rotatory strength), \mathbf{D}_j and \mathbf{M}_j are electric and magnetic transition dipole moments, and ω_j are excitation frequencies. OR is particularly sensitive to approximations because the R_j depend on the magnitudes of both transition dipoles and the angle between them.

A recent OR benchmark³⁵ on average did not show improvements from RSE functionals over global hybrids when assessed by experimental solution-phase data. We subsequently investigated IP-tuned LC functionals²¹ and compared them with WFT. Examples are shown in Figure 11. For β -pinene, a very problematic case for OR, there is considerable improvement from tuning, going hand in hand with a small DE. We cautiously recommend IP-tuned functionals for OR because of such improvements without finding too much deterioration for other molecules.

Norbornenone (Figure 12) has an exceptionally large isotropic OR given its size, $[\phi]_D \approx -816$ in vapor phase.³⁷ Similar bicyclic molecules with a carbonyl or C=C group, but not both, exhibit one to 2 orders of magnitude smaller ORs.

methylloxirane	λ [nm]	$[\phi]_D$		
		CCSD	LC-PBE0	LC-PBE0*
	355	-32.8	-21.60	-19.84
	589.3	-17.5	-11.22	-11.23
	633	-15.4	-9.874	-9.908

β -pinene	λ [nm]	$[\phi]_D$		
		CCSD	LC-PBE0	LC-PBE0*
	355	115.4	45.32	123.2
	589.3	1.0	-11.06	1.751
	633	-1.0	-10.72	-0.234

ethynyl[6]helicene	CC2	$[\phi]_D$	
		LC-PBE0	LC-PBE0*
		-14799	
		-13183	
		-17245	

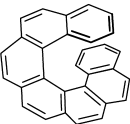
[7]helicene	CC2	$[\phi]_D$	
		LC-PBE0	LC-PBE0*
		-18226	
		-15108	
		-19980	

Figure 11. Molar rotations (deg cm²/dmol) for selected compounds.²¹ LC-PBE0 with $\gamma = 0.3$, IP-tuned LC-PBE0*, and WFT reference data.

Furthermore, with TD-KST the calculated OR is dramatically dependent on the functional, as seen in Table 5 and by the varying extensions of the OR tensor plots in Figure 12. CC theory³⁷ and a 2DT LC-PBEh* functional³⁶ bracket the gas-phase experimental OR from below and above, respectively, in terms of magnitude.

An OR tensor analysis in terms of LMOs exposed the reasons for the strong functional dependence and why the OR is so large.³⁶ The $\pi(\text{C}=\text{C})$ orbital is delocalized over to the carbonyl group, and the non-bonding carbonyl oxygen LP $n(\text{C}=\text{O})$ is also significantly delocalized (Table 5), indicating an electronic coupling whose relative functional dependence is large and correlates with the OR magnitude. Below the equation inset in Figure 12 are isosurfaces of OR densities for $\pi(\text{C}=\text{C})$ and $n(\text{C}=\text{O})$ after 2DT. The densities integrate to

Table 5. Norbornenone:³⁶ Percent of Density of $\pi(\text{C}=\text{C})$ and $n(\text{C}=\text{O})$ Associated with the Carbonyl Carbon, and Calculated Molar Rotation

	$\pi(\text{C}=\text{C})$	$n(\text{C}=\text{O})$	$-[\phi]_D$
HF	0.62	2.60	646
LC-PBEh* ^a	0.71	3.18	920
B3LYP	0.80	3.42	1291
PBE	0.90	3.81	1932

^a2DT parametrization.

large OR contributions per LMO. The electronic coupling causes visibly large OR density values for $\pi(\text{C}=\text{C})$ around the carbonyl group and vice versa for $n(\text{C}=\text{O})$, which are reinforcing and responsible for the particularly large OR. Furthermore, these delocalization contributions become much larger for functionals with large DE and much smaller for HF, linking the magnitude of the OR and the functional sensitivity directly to the DE.³⁶

3.6. Hyperpolarizabilities of Push–Pull π -Systems and CT Excitations

Researchers have long been interested in calculating NLO properties to assist the design of NLO materials.³⁸ Figure 13 displays static first hyperpolarizabilities $\beta_{||}$ parallel to the permanent dipole moment for selected organic push–pull chromophores.⁷ The calculations can be assessed by comparison with MP2.³⁸ The HF–MP2 comparison demonstrates the importance of electron correlation for the longer chains. KST with standard functionals is plagued by large DEs and too low CT excitations,⁷ causing a severe overestimation of $\beta_{||}$. IP-tuned LC functionals performed well in comparison. Their superior performance can be linked to the calculated CT energy (Table 4, Figure 1). In a two-level model, $\beta_{||} \propto E_{\text{CT}}^{-2}$, meaning that the CT problem can have disastrous consequences. The performance of KST for $\beta_{||}$ follows closely the extent of $E(\Delta N)$ curvatures and associated LMO delocalization.⁷

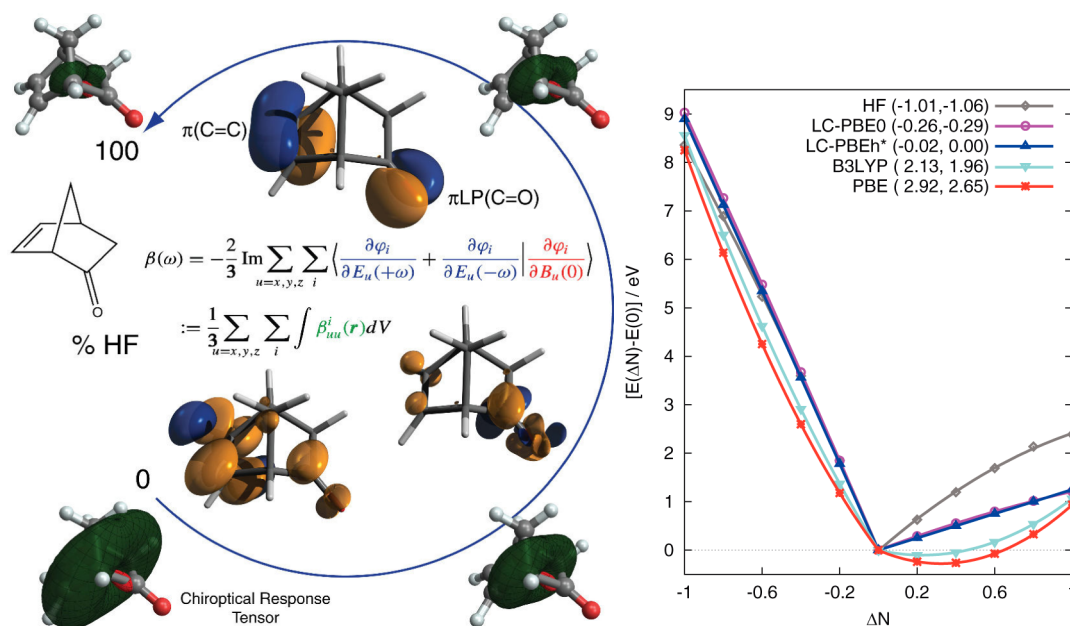


Figure 12. Norbornenone.³⁶ (left) KST OR tensors (green/red) versus % eX. (top center) Two LMOs representing $\pi(\text{C}=\text{C})$ and $n(\text{C}=\text{O})$. (equation and isosurface plots below) OR densities for $\pi(\text{C}=\text{C})$ and $n(\text{C}=\text{O})$ for 2DT LC-PBEh*. (right) Curvature of $E(N)$.

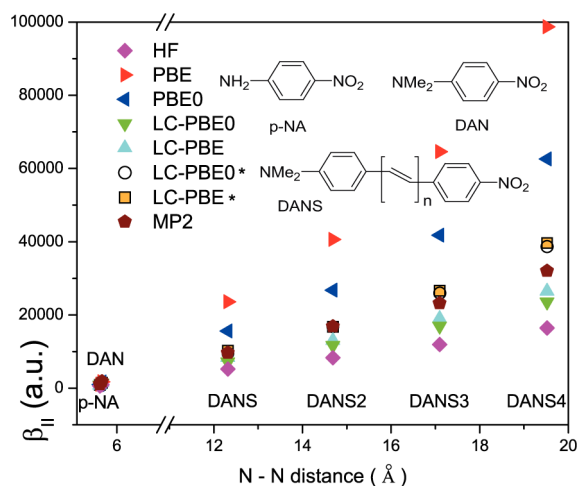


Figure 13. Static hyperpolarizability (β_{\parallel}) for p-NA, DAN, DANS, and derivatives with $n > 1$.⁷ IP-tuned LC-PBE0* and LC-PBE*.

3.7. Band Gaps and 0–0 Transitions

For many potential applications, “band gap engineering” is critical for chromophores. In a recent study, IP-tuned LC functionals produced overall reliable vertical IPs, EAs, fundamental gaps ΔE_F , and optical gaps ΔE_O , for conducting oligomers of varying lengths.²⁴ Figure 14 displays representa-

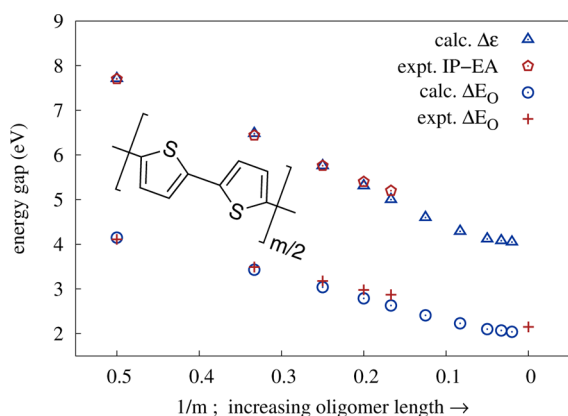


Figure 14. Experimental $\Delta E_F = \text{IP} - \text{EA}$ and ΔE_O of thiophene- m -mers. Calculated orbital energy gap $\Delta \epsilon$ and TD-KST singlet excitation energy from IP-tuned LC-PBE0*.²⁴

tive data for oligo-thiophene. Standard functionals gave rather severe DEs causing CT-like problems with the optical gaps. We note in passing that 2DT has been employed to match KST orbital energies of polyaromatic hydrocarbons with GW many-body quasi-particle spectra.²⁵

Finally, a comparison of mean absolute errors for 0–0 transitions for 40 π -conjugated dyes³⁹ is shown in Figure 15. IP-tuned LC-PBE* produced the smallest deviations from experiment among the tested functionals and a high correlation of $R = 0.93$.

4. OUTLOOK

Electronic structure methods should ideally be universal. Therefore, molecule-specific parameters for KST calculations are not particularly satisfying, for example, they break size-extensivity.²⁸ However, for spectra, ground-state, and response properties the improvements can be dramatic. Among the

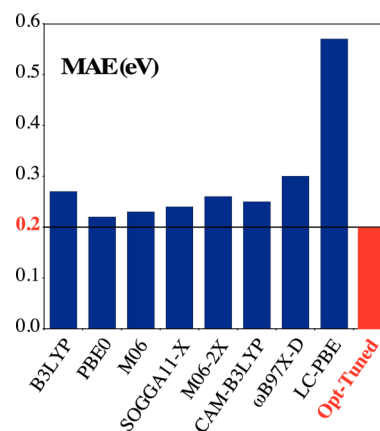


Figure 15. Mean absolute deviation of calculated 0–0 $S_0 - S_1$ excitation energies from experiment for 40 conjugated organic dyes.³⁹ “Opt-Tuned” = IP-tuned LC-PBE*.

indicators for whether a calculated property is likely to improve may be low-energy CT excitations in the electronic spectrum or when an LMO analysis of the property with different types of standard functionals reveals a sensitivity to the extent of orbital delocalization. Tuning may be unsuccessful because of insufficient dynamic correlation from the functional or multireference character of the electronic state. Dispersion interactions may need to be treated explicitly.⁴⁰ Nonempirical universal KST methods beyond Perdew’s rung 3 and 4 might eventually replace the need for tuned functionals. In the meantime, there is considerable value in using IP-tuning and DE-minimization concepts as diagnostics and to improve calculations of spectroscopic and optical properties at comparatively low computational cost.

■ ASSOCIATED CONTENT

Supporting Information

Definitions of acronyms and additional details regarding sections 1 and 2. This material is available free of charge via the Internet at <http://pubs.acs.org>.

■ AUTHOR INFORMATION

Corresponding Author

*email: jochena@buffalo.edu.

Funding

Studies of organic molecules have been supported by NSF Grant CHE-1265833. Development of fractional electron number KST functionality and paramagnetic NMR studies have been supported by the DOE, Basic Energy Sciences, Heavy Element Chemistry, Grant DE-FG02-09ER16066. M.S. acknowledges the FNP Homing Plus programme cofinanced by EU funds and a Ministry of Science and Higher Education in Poland scholarship.

Notes

The authors declare no competing financial interest.

Biographies

Jochen Autschbach (b. Germany 1968) obtained his Ph.D. from the University of Siegen in 1999. He joined the Department of Chemistry at the University at Buffalo in 2003 and became Full Professor in 2009. Jochen’s research is focused on response properties of molecules and extended systems, dynamic phenomena, and relativistic quantum

chemistry, with applications in spectroscopy, magnetic resonance, optical activity, and nonlinear optics.

Monika Srebro (b. Poland 1982) received a theoretical chemistry Ph.D. from the Jagiellonian University, Krakow, Poland, in 2010 and was a postdoctoral fellow in Jochen Autschbach's group in 2011–2012. She holds an academic position in the Faculty of Chemistry at Jagiellonian University. Her research interests are electronic structure–bonding–properties relationships of transition-metal based materials.

REFERENCES

- (1) Kohn, W.; Sham, L. Self-Consistent Equations Including Exchange and Correlation Effects. *Phys. Rev. A* **1965**, *140*, 1133–1138.
- (2) Perdew, J. P.; Ruzsinszky, A.; Constantin, L. A.; Sun, J.; Csonka, G. I. Some Fundamental Issues in Ground-State Density Functional Theory: A Guide for the Perplexed. *J. Chem. Theory Comput.* **2009**, *5*, 902–908.
- (3) Marques, M. A. L.; Ullrich, C. A.; Nogueira, F.; Rubio, A.; Burke, K.; Gross, E. K. U., Eds.; *Time-Dependent Density Functional Theory*; Vol. 706 of Lecture Notes in Physics; Springer: Berlin, 2006.
- (4) Cohen, A. J.; Mori-Sánchez, P.; Yang, W. Challenges for Density Functional Theory. *Chem. Rev.* **2012**, *112*, 289–320.
- (5) Dreuw, A.; Weisman, J. L.; Head-Gordon, M. Long-Range Charge-Transfer Excited States in Time-Dependent Density Functional Theory Require Non-local Exchange. *J. Chem. Phys.* **2003**, *119*, 2943–2946.
- (6) Autschbach, J. Charge-Transfer Excitations and Time-Dependent Density Functional Theory: Problems and Some Proposed Solutions. *ChemPhysChem* **2009**, *10*, 1757–1760.
- (7) Sun, H.; Autschbach, J. Influence of the Delocalization Error and Applicability of Optimal Functional Tuning in Density Functional Calculations of Nonlinear Optical Properties of Organic Donor/Acceptor Chromophores. *ChemPhysChem* **2013**, *14*, 2450–2461.
- (8) Tozer, D. J. Relationship between Long-Range Charge-Transfer Excitation Energy Error and Integer Discontinuity in Kohn-Sham Theory. *J. Chem. Phys.* **2003**, *119*, 12697–12699.
- (9) Maitra, N. T.; Tempel, D. G. Long-Range Excitations in Time-Dependent Density Functional Theory. *J. Chem. Phys.* **2006**, *125*, No. 184111.
- (10) Iikura, H.; Tsuneda, T.; Yanai, T.; Hirao, K. A Long-Range Correction Scheme for Generalized-Gradient-Approximation Exchange Functionals. *J. Chem. Phys.* **2001**, *115*, 3540–3544.
- (11) Yanai, T.; Tew, D. P.; Handy, N. C. A New Hybrid Exchange-Correlation Functional Using the Coulomb-Attenuating Method (CAM-B3LYP). *Chem. Phys. Lett.* **2004**, *393*, 51–57.
- (12) Tawada, Y.; Tsuneda, T.; Yanagisawa, S.; Yanai, T.; Hirao, K. A Long-Range-Corrected Time-Dependent Density Functional Theory. *J. Chem. Phys.* **2004**, *120*, 8425–8433.
- (13) Rohrdanz, M. A.; Herbert, J. M. Simultaneous Benchmarking of Ground- and Excited-State Properties with Long-Range-Corrected Density Functional Theory. *J. Chem. Phys.* **2008**, *129*, No. 034107.
- (14) Baer, R.; Livshits, E.; Salzner, U. Tuned Range-Separated Hybrids in Density Functional Theory. *Annu. Rev. Phys. Chem.* **2010**, *61*, 85–109.
- (15) Stein, T.; Kronik, L.; Baer, R. Reliable Prediction of Charge Transfer Excitations in Molecular Complexes Using Time-Dependent Density Functional Theory. *J. Am. Chem. Soc.* **2009**, *131*, 2818–2820.
- (16) Kuritz, N.; Stein, T.; Baer, R.; Kronik, L. Charge-Transfer-Like $\pi \rightarrow \pi^*$ Excitations in Time-Dependent Density Functional Theory: A Conundrum and Its Solution. *J. Chem. Theory Comput.* **2011**, *7*, 2408–2415.
- (17) Körzdörfer, T.; Sears, J. S.; Sutton, C.; Brédas, J.-L. Long-Range Corrected Hybrid Functionals for π -Conjugated Systems: Dependence of the Range-Separation Parameter on Conjugation Length. *J. Chem. Phys.* **2011**, *135*, No. 204107.
- (18) Kronik, L.; Stein, T.; Refaely-Abramson, S.; Baer, R. Excitation Gaps of Finite-Sized Systems from Optimally Tuned Range-Separated Hybrid Functionals. *J. Chem. Theory Comput.* **2012**, *8*, 1515–1531.
- (19) Foster, M. E.; Wong, B. M. Nonempirically Tuned Range-Separated DFT Accurately Predicts Both Fundamental and Excitation Gaps in DNA and RNA Nucleobases. *J. Chem. Theory Comput.* **2012**, *8*, 2682–2687.
- (20) Vydrov, O. A.; Scuseria, G. E.; Perdew, J. P. Tests of Functionals for Systems with Fractional Electron Number. *J. Chem. Phys.* **2007**, *126*, No. 154109.
- (21) Srebro, M.; Autschbach, J. Tuned Range-Separated Time-Dependent Density Functional Theory Applied to Optical Rotation. *J. Chem. Theory Comput.* **2012**, *8*, 245–256.
- (22) Moore, B. II; Autschbach, J. Density Functional Study of Tetraphenylporphyrin Long-Range Exciton Coupling. *ChemistryOpen* **2012**, *1*, 184–194.
- (23) Srebro, M.; Autschbach, J. Does a Molecule-Specific Density Functional Give an Accurate Electron Density? The Challenging Case of the CuCl Electric Field Gradient. *J. Phys. Chem. Lett.* **2012**, *3*, 576–581.
- (24) Sun, H.; Autschbach, J. Electronic Energy Gaps for π -Conjugated Oligomers and Polymers Calculated with Density Functional Theory. *J. Chem. Theory Comput.* **2014**, *10*, 1035–1047.
- (25) Refaely-Abramson, S.; Sharifzadeh, S.; Govind, N.; Autschbach, J.; Neaton, J. B.; Baer, R.; Kronik, L. Quasiparticle Spectra from a Non-empirical Optimally-Tuned Range-Separated Hybrid Density Functional. *Phys. Rev. Lett.* **2012**, *109*, No. 226405.
- (26) Johnson, E. R.; Otero de-la Roza, A.; Dale, S. G. Extreme Density-Driven Delocalization Error for a Model Solvated-Electron System. *J. Chem. Phys.* **2013**, *139*, No. 184116.
- (27) Schwerdtfeger, P.; Pernpointner, M.; Nazarewicz, W. Calculation of Nuclear Quadrupole Coupling Constants. In *Calculation of NMR and EPR Parameters. Theory and Applications*; Kaupp, M., Bühl, M., Malkin, V. G., Eds.; Wiley-VCH: Weinheim, Germany, 2004; pp 279–291.
- (28) Karolewski, A.; Kronik, L.; Kümmel, S. Using Optimally Tuned Range Separated Hybrid Functionals in Ground-State Calculations: Consequences and Caveats. *J. Chem. Phys.* **2013**, *138*, No. 204115.
- (29) Pritchard, B.; Autschbach, J. Theoretical Investigation of Paramagnetic NMR Shifts in Transition Metal Acetylacetonato Complexes: Analysis of Signs, Magnitudes, and the Role of the Covalency of Ligand-Metal Bonding. *Inorg. Chem.* **2012**, *51*, 8340–8351.
- (30) Jacquemin, D.; Zhao, Y.; Valero, R.; Adamo, C.; Ciofini, I.; Truhlar, D. G. Verdict: Time-Dependent Density Functional Theory Not Guilty of Large Errors for Cyanines. *J. Chem. Theory Comput.* **2012**, *8*, 1255–1259.
- (31) Moore, B. II; Autschbach, J. Longest-Wavelength Electronic Excitations of Linear Cyanines: The Role of Electron Delocalization and of Approximations in Time-Dependent Density Functional Theory. *J. Chem. Theory Comput.* **2013**, *9*, 4991–5003.
- (32) Matile, S.; Berova, N.; Nakanishi, K.; Fleischhauer, J.; Woody, R. W. Structural Studies by Exciton Coupled Circular Dichroism over a Large Distance: Porphyrin Derivatives of Steroids, Dimeric Steroids, and Brevetoxin B. *J. Am. Chem. Soc.* **1996**, *118*, 5198–5206.
- (33) Polavarapu, P. L. Renaissance in Chiroptical Spectroscopic Methods for Molecular Structure Determination. *Chem. Rec.* **2007**, *7*, 125–136.
- (34) Autschbach, J. Introduction to the Computation of Chiroptical Properties with First-Principles Theoretical Methods: Background and Illustrative Examples. *Chirality* **2009**, *21*, E116–E152.
- (35) Srebro, M.; Govind, N.; de Jong, W.; Autschbach, J. Optical Rotation Calculated with Time-Dependent Density Functional Theory: The OR45 benchmark. *J. Phys. Chem. A* **2011**, *115*, 10930–10949.
- (36) Moore, B. II; Srebro, M.; Autschbach, J. Analysis of Optical Activity in Terms of Bonds and Lone-Pairs: The Exceptionally Large Optical Rotation of Norbornenone. *J. Chem. Theory Comput.* **2012**, *8*, 4336–4346.
- (37) Lahiri, P.; Wiberg, K. B.; Vaccaro, P. H.; Caricato, M.; Crawford, T. D. Large Solvation Effect in the Optical Rotatory Dispersion of Norbornenone. *Angew. Chem., Int. Ed.* **2014**, *53*, 1386–1389.

(38) Champagne, B.; Perpète, E.; Jacquemin, D.; van Gisbergen, S. J. A.; Baerends, E. J.; Soubra-Ghaoui, C.; Robins, K. A.; Kirtman, B. Assessment of Conventional Density Functional Schemes for Computing the Dipole Moment and (Hyper)Polarizabilities of Push-Pull π -Conjugated Systems. *J. Phys. Chem. A* **2000**, *104*, 4755–4763.

(39) Jacquemin, D.; Moore, B. II; Planchat, A.; Adamo, C.; Autschbach, J. Performance of an Optimally-Tuned Range-Separated Hybrid Functional for 0–0 Electronic Excitation Energies. *J. Chem. Theory Comput.* **2014**, *10*, 1677–1685.

(40) Agrawal, P.; Tkatchenko, A.; Kronik, L. Pair-Wise and Many-Body Dispersive Interactions Coupled to an Optimally Tuned Range-Separated Hybrid Functional. *J. Chem. Theory Comput.* **2013**, *9*, 3473–3478.